IEEE Access
Multidisciplinary ⋮ Rapid Review ⋮ Open Access Journal

Received November 8, 2019, accepted November 17, 2019, date of publication November 19, 2019,
date of current version December 2, 2019.

Digital Object Identifier 10.1109/ACCESS.2019.2954457

White Blood Cell Segmentation via Sparsity and Geometry Constraints

ZHEN ZHONG[1,2], TAO WANG[1,3,4], KUN ZENG[1], XIAOGEN ZHOU[3], AND ZUOYONG LI[1,2]

[1]Fujian Provincial Key Laboratory of Information Processing and Intelligent Control, Minjiang University, Fuzhou 350108, China
[2]Department of Traditional Chinese Medicine, Fujian University of Traditional Chinese Medicine, Fuzhou 350108, China
[3]College of Mathematics and Computer Science, Fuzhou University, Fuzhou 350108, China
[4]NetDragon Inc., Fuzhou 350001, China

Corresponding author: Tao Wang (taowang2600@gmail.com)

This work was supported in part by the NSFC under Grant 61703195, Grant 61702431, Grant 61972187, and Grant 61772254, in part by the Fujian NSF under Grant 2019J01756, in part by the Key Project of College Youth NSF of Fujian Province under Grant JZ160467, in part by The Education Department of Fujian Province under Grant JAT170459 and Grant JK2017039, in part by the Distinguished Young Scholars Program of Fujian Universities, in part by the Fuzhou Technology Planning Program under Grant 2018-G-96 and Grant 2018-G-98, in part by Minjiang University under Grant MJUKF201716, Grant MJY19021, and Grant MJY19022, and in part by the Fujian University of Traditional Chinese Medicine under Grant X2017004-platform.

ABSTRACT Digital pathology and microscopic image analysis play an important role in cell morphology research. In particular, the effective segmentation of White Blood Cells (WBCs) remains a challenging problem due to the blurring boundaries of WBCs under rapid staining, as well as the adhesion between leukocytes and other cells. In this paper, we propose a novel WBC (including nuclei and cells) segmentation algorithm based on both sparsity and geometry constraints. Specifically, we first construct a sparse image representation via combining the HSL color space and the RGB color channels, followed by the use of a sparsity constraint to only preserve useful information from the nuclei features. In addition, we introduce a robust model fitting strategy (i.e., the geometry constraint) to detect cells. Our model fitting strategy is able to significantly improve the robustness of the proposed segmentation algorithm against outliers that could seriously contaminate WBCs. The experimental results show that the proposed algorithm presents clear advantages over the state-of-the-art WBC segmentation algorithms in terms of accuracy.

INDEX TERMS Geometry constraint, sparsity constraint, white blood cell segmentation.

I. INTRODUCTION

White blood cells (WBCs) [1], [2] are important defense cells in human blood that consists of five kinds of cells, i.e., neutrophils, basophils, eosinophils, monocytes, and lymphocytes. The WBC segmentation is a challenging task for a variety of medical diagnosis applications. For example, the visual examination of WBCs in blood smears collected under a bright field microscope can be used to diagnose various diseases, such as septic bacterial inflammation, uremia, and various kinds of leukaemia.

A number of WBC segmentation methods have been proposed in recent years. In general, existing methods can be divided into two distinct categories: supervised vs. unsupervised WBC segmentation methods. The supervised WBC segmentation methods [3]–[6] formulate the WBC segmentation problem as a multi-class classification problem. They are typically solved in a two-step manner, i.e., first extracting image features and then classifying the extracted features. However, these supervised methods require a large number of annotated training samples, which are often manually labeled and difficult to obtain. Particularly, the manual pixelwise segmentation process is tedious and error-prone for the abundant fine structures in the blood cell imagery. In addition, the training and test images are assumed to be visually similar to minimize the domain shift between training and test images. In practice, this assumption could negatively impact the generalization abilities of these supervised algorithms.

One appealing alternative to the supervised methods is the unsupervised WBC segmentation methods (e.g., thresholding [7]–[9], K-means [10], [11], fuzzy C-means (FCM) [12] and mean shift [13]) that do not generally require manually labeled images. Indeed, blood cells exhibit strong overall

The associate editor coordinating the review of this manuscript and approving it for publication was Leyi Wei.

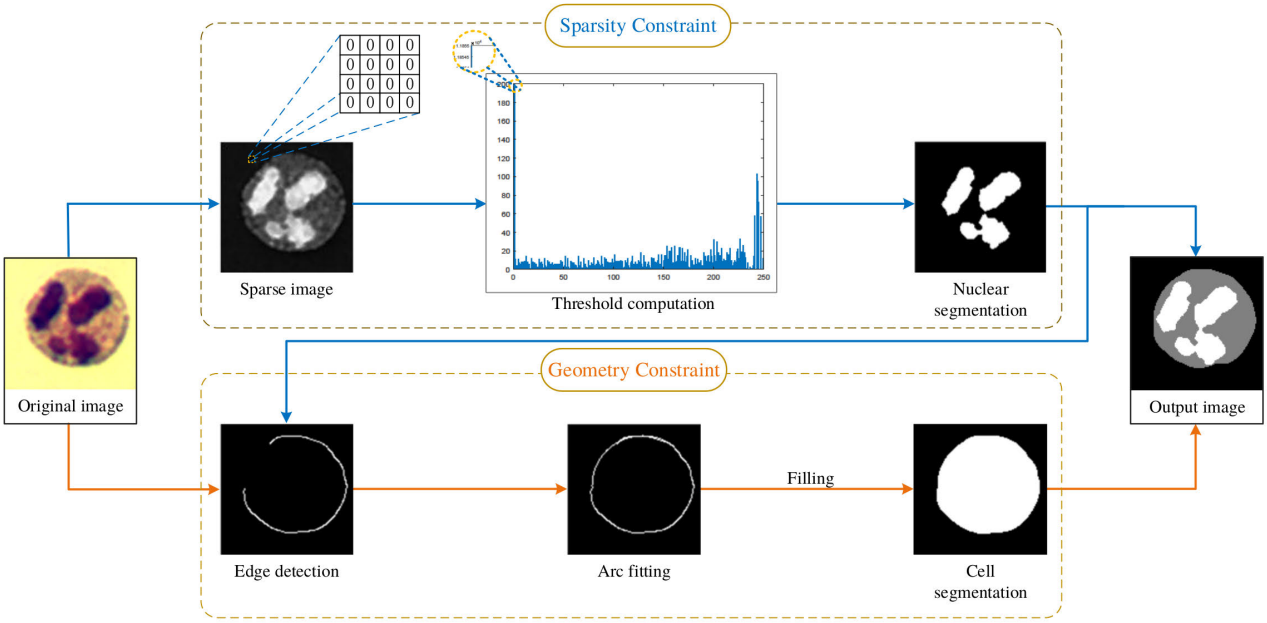

FIGURE 1. Overview of the proposed algorithm. Segmentation of WBCs are obtained via two streams by applying a sparsity constraint (top) and a geometry constraint (bottom) respectively. The sparsity constraint augments the image features for accurate nuclear segmentation. The geometry constraint uses arc fitting to complete the partial cell boundary derived from the original image and the nuclear segmentation results. See text for details.

shape priors and internal structural patterns that may render training a data-hungry discriminative segmentation model unnecessary. One of the key challenges, however, is that WBCs and RBCs (i.e., red blood cells) often adhere together since they have similar colors. Such ambiguity presents a unique challenge for the accurate localization and the delineation of WBCs using unannotated images only. In particular, it is difficult to obtain pixel accurate cell segmentations when the boundary information is weak, and this leads to spurious or eroded segmentations as illustrated in Fig. 6 and Fig. 7.

To address the above issues, we propose a novel WBC segmentation algorithm based on both the sparsity and the geometry constraints, as shown in Fig. 1. Our primary goal is to reduce the impact of WBC and RBC adhesions and WBC boundary ambiguities for WBC segmentation. To achieve this, we adopt a two-stream architecture that incorporates sparsity and geometry cues respectively. Specifically, we first use the HSL color space and the RGB color channels to construct an image representation that makes the features of the nuclei more significant. Afterwards, we use the sparsity constraint to preserve only the nuclei features to obtain a nuclear segmentation. The preserved features are also used as an input to the geometry stream to identify nuclei regions that are irrelevant for cell boundary segmentation. In the geometry stream, our goal is to extract the cell boundaries, beginning with edge detection. Note that, the edge detection results are generally composed of incomplete boundary fragments. Therefore, we introduce a robust arc fitting strategy to complete the WBC boundaries. Importantly, the model fitting process allows us to recover weak or ambiguous boundary information and to propose cell structures from partial observations only. The overview of the proposed algorithm is presented in Fig. 1.

Key contributions of this paper are summarized as follows:

- We construct a new sparse image representation based on the HSL color space and the RGB color channels for nuclear segmentation. The constructed sparse image representation is able to emphasize on key structures while weakening irrelevant features (e.g., backgrounds, red blood cells, cytoplasms).
- We propose a model fitting strategy to improve the robustness and effectiveness of WBC segmentation for detecting incomplete cell boundaries. To the best of our knowledge, this model fitting based algorithm for addressing the WBC segmentation problem has not yet been reported.
- Experimental results demonstrate that the proposed algorithm is able to achieve highly accurate results on both rapid and standard staining WBC data. When compared to several other state-of-the-art WBC segmentation algorithms (e.g., Combination Graph Segmentation (CGS) [8], Watershed Segmentation (WS) [14], Support Vector Machines (SVM) [3] and Adaptive Histogram Threshold segmentation (AHT) [9]), the proposed algorithm exhibits a significant superiority in terms of the segmentation accuracy.

The rest of the paper is organized as follows. In Section 2, we discuss the recent literature on WBC segmentation. We present the details of the sparsity and geometry constraints to segment WBCs in Section 3. In Section 4,

we compare our algorithm with the state-of-the-art WBC segmentation algorithms. We summarize this paper with some closing remarks in Section 5.

II. RELATED WORK

In this section, we briefly review the existing literature on WBC segmentation. As discussed in the previous section, we broadly categorize existing WBC segmentation methods into two distinct groups: the supervised methods and the unsupervised methods.

The supervised methods include those based on support vector machines (SVMs) [3], [15] and convolutional neural nets (CNNs) [2], [4]–[6], [16]–[20], among others. For example, Zheng *et al.* [3] first use an EM algorithm-based layered sampling technique to sample the images. Afterwards, they train an SVM online by using the color features of the sampled pixels, and then classify each pixel in the test image by the SVM. Inspired by the recent success of CNNs in image classification and segmentation, many recent papers [2], [4]–[6], [16]–[20] propose to solve the WBC segmentation or similar medical imaging problems by training a special purpose CNN. For example, Shitong *et al.* [2] propose a fuzzy cellular neural net for white blood cell detection and segmentation. More recently, Habibzadeh *et al.* [16] propose to use pre-trained deep neural nets for white blood cell classification. In addition, Tiwari *et al.* [17] propose a 6-layer CNN for detecting subtypes of blood cells. We note that CNN-based methods generally require a large amount labeled training data, which may be prohibitive to obtain especially in the medical imaging domains. Contrary to supervised methods, we explore improving the localization accuracy of unsupervised WBC segmentation methods by exploiting sparsity in image features and the geometric regularities (e.g., shape priors) of blood cells.

The unsupervised methods include threshold-based segmentation [7]–[9], cluster-based methods [10], [13], and the watershed algorithm based methods [14], [21], etc. For example, Nee *et al.* [7] propose to use gradient magnitude, thresholding, morphological operations and the watershed transform to perform cell segmentation. Zhang *et al.* [10] first convert the color space of the WBC images, and then use K-means to segment the color space decomposition. In addition, Liu *et al.* [13] use the mean shift algorithm instead of K-means to obtain whole cells, and then use the watershed algorithm to segment cells accurately. Furthermore, Arslan *et al.* [14] model color and shape characteristics of WBCs by defining two transformations, and then use the watershed algorithm for effective segmentation. In general, unsupervised methods do not require a large number of annotated training data. However, they are prone to overfitting/underfitting when the color and shape variations of cells are large. Therefore, a large number of adjustments to parameters may be required. In addition, RBCs are often stuck to and being visually similar to WBCs, making the WBC segmentation problem more challenging when RBCs and other staining impurities are present. In this paper, we propose exploiting a sparse image representation based on the HSL color space and the RGB color channels. Such a representation can effectively distinguish WBCs from RBCs. In order to deal with weak or ambiguous boundaries in original images, we also introduce a robust model fitting strategy to detect incomplete cells from partial observations.

III. THE PROPOSED ALGORITHM

In this section, we describe the details of the proposed WBC segmentation algorithm based on sparsity and geometry constraints. Specifically, in the first step, we segment the nuclei by a sparsity constraint. We adopt an image representation that makes the features of nuclei more significant, and therefore can be reliably detected. In the second step, we use a geometry constraint to detect cells. The key idea in this step involves the use of a model fitting procedure to recover cells from weak and incomplete boundaries.

A. NUCLEUS SEGMENTATION BASED ON SPARSITY CONSTRAINT

The nucleus is the largest and the most important cellular structure in a WBC and is also the regulatory center for cytogenetics and metabolism. Accurate segmentation of the nucleus is an important step in the segmentation of WBCs. In our algorithm, nucleus segmentation involves two main stages: 1) constructing a sparse image representation based on the HSL color space and the RGB color channels; 2) segmenting the nucleus by a sparsity constraint.

1) CONSTRUCTING A SPARSE IMAGE REPRESENTATION

The HSL color space [22] is a way of reflecting the perceived colors of the human vision system. Compared to the most widely used RGB imagery, the three channels in HSL, i.e., hue, saturation, and lightness are a more natural representation of the visual perception in human eyes. More importantly, the rapidly stained blood cell image shown in Fig. 2 has different intensity values in the HSL color space and the RGB color channels. In particular, the nucleus is darker than surrounding pixels in the G and B channels, and brighter in the S channel. Therefore, we would like to exploit these cues to obtain an image that highlights the nucleus to improve the accuracy of threshold-based segmentation. Based on our empirical observations and initial experiments, we have found a specific combination of channels that is able to highlight the nucleus. The output image from this processing, I_s, can be given by:

$$I_s(I_{in}) = S - 2 \times G + 2 \times B + \frac{S - G}{B} \tag{1}$$

where I_{in}, S, G and B denotes the input image, saturation, green and blue channel maps, respectively.

2) THE SPARSITY CONSTRAINT

In the next step, we obtain the intensity histogram of I_s and then perform automatic threshold segmentation [23].

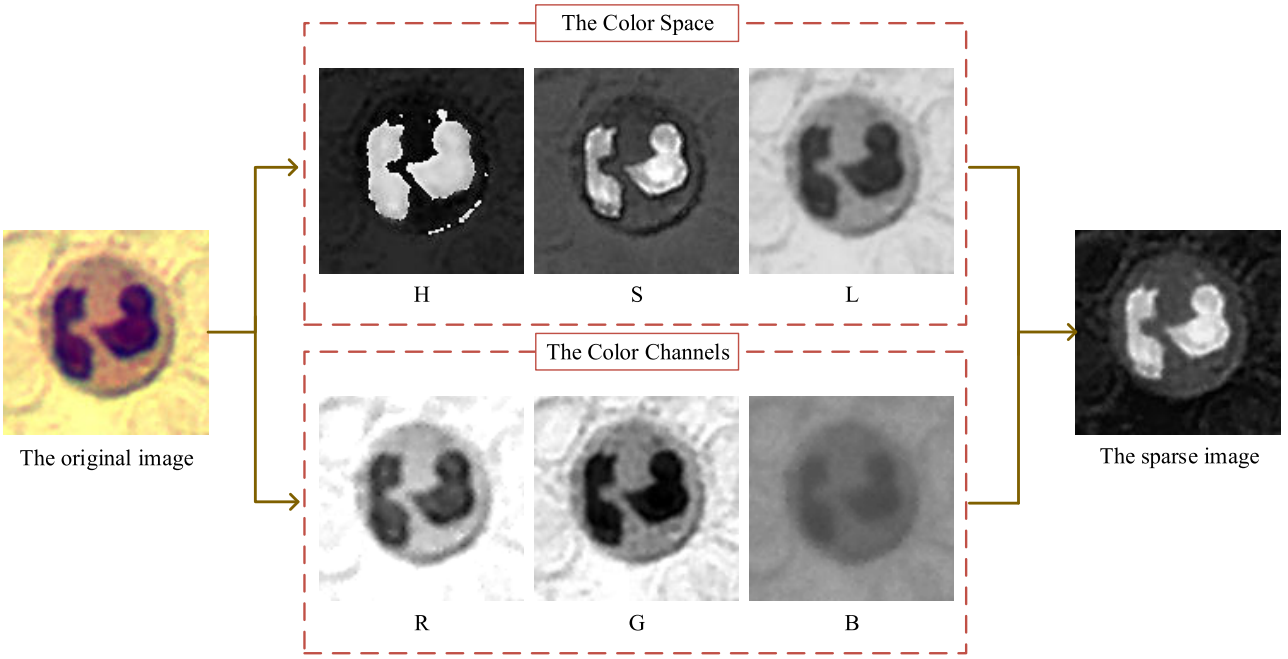

FIGURE 2. An example of a WBC image under rapid staining. We show the image in both the HSL and RGB color spaces. Note that the nucleus has lower intensity values (i.e., darker) in some channels, and we exploit these cues for reliable nuclear segmentation. See text for details.

As shown in the upper part of Fig. 1, we first obtain the first two peaks T_1, T_2 in the histogram, and then find the lowest point between the two peaks, and T is our segmentation threshold:

$$T = \min[T_1, T_2] \tag{2}$$

Then we obtain the nucleus region $C_n(i, j)$ by T:

$$C_n(i,j) = \begin{cases} 1 & \text{if } I_s(i,j) \geq T \\ 0 & \text{otherwise} \end{cases} \tag{3}$$

where $C_n(i, j)$ denote a binary map for nuclear segmentation. In addition, we perform the connected component analysis [24] to remove small and isolated noise pixels.

B. CELL SEGMENTATION BASED ON GEOMETRY CONSTRAINT

In this section, we extract the geometric features of the cells by edge detection, and then we propose a new model fitting strategy for geometric features (note that robust model fitting can extract valid information from a large amounts of outliers [25]–[29]). In particular, the edge detection results typically contain incomplete boundary fragments, and our model fitting approach aims at recovering ambiguous or weak cell boundaries for accurate localization.

1) OVERVIEW OF THE PROPOSED MODEL FITTING STRATEGY

The core idea of RANSAC [30], which is the most popular model fitting method, is to find the most suitable model by generating a large number of model candidates, which is often very time-consuming. We note that edge detection algorithms usually cannot fully recover WBC boundaries. That is, there exists a gap when we obtain the edge features from a WBC image. To address this issue, we use the detected edges to infer the missing parts. Specifically, we use the edges to infer an underlying model (i.e., a circle) that closes the gaps in between boundary fragments. Note that, if we use RANSAC to detect the cells directly, it always fits the best circle, but not the best arc we need in order to fill in the missing parts of cell boundaries. Our strategy makes use of the strong shape priors of cells and respects the non-circular boundary detection results. On one hand, stronger boundaries that can be detected will be retained. On the other hand, any missing cell boundaries will be filled in with an underlying circle that best fits the detectable parts of the cell boundaries. In our method, instead of fitting the entirety of the cell boundaries in RANSAC, we only fill in gaps in incomplete boundaries with the most appropriate arc, and then we use this arc to close the gap. In addition, we fit the circles in RANSAC with two breakpoints of a boundary fragment to make sure that the fitted arc can be seamlessly stitched back to the detected parts of the boundary. We show the flow chart of the proposed model fitting strategy in Fig. 3.

2) THE PRETREATMENT STEP

As a preprocessing step, we would like to remove the red blood cells and some other backgrounds irrelevant to WBC segmentation. We do so by carefully examining the colors of various regions in both the rapid staining and standard staining images, as shown in Fig. 4. Specifically, we make the following observations:

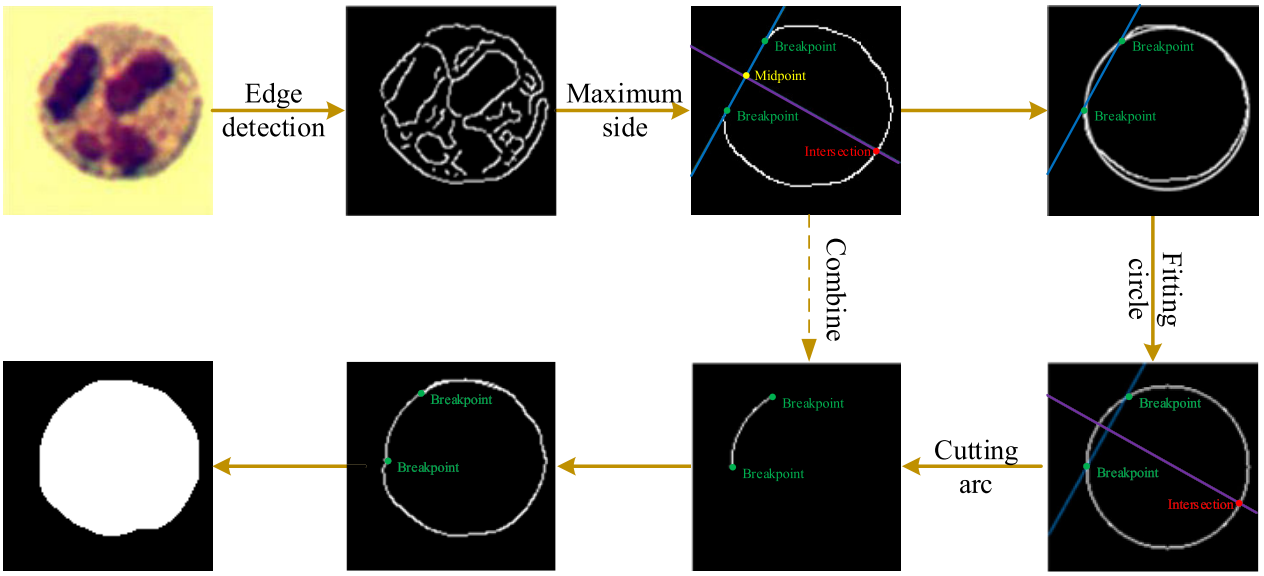

FIGURE 3. Flow chart of the proposed model fitting strategy. We first retain only the longest boundary fragment, which typically belongs to the outer boundary of the WBC. Afterwards, we fit an arc with two breakpoints plus another random point from the fragment. A number of arc hypotheses are generated and the best is chosen. The best arc is then stitched back to the fragment, resulting in a complete and closed WBC boundary. See text for details.

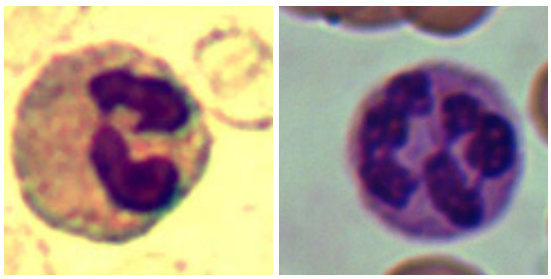

(a) (b)

FIGURE 4. Cell examples in the pretreatment step. (a) WBC under rapid staining, and (b) standard stained WBC. We note that although the background colors are different, in both images the backgrounds have high intensity values in the green channel. Therefore, we use color cues for background removal. See text for details.

- The background under rapid staining is yellow, and the background under standard staining is green.
- For both rapid and standard staining images, the backgrounds have high intensity values in the green channel. In addition, red blood cells have high intensity values in the red channel.

Therefore, we can ignore image pixels that have high intensities in the red and the green channels, as follows:

- If the green channel intensity is greater than the green channel threshold $t_1(i,j)$, we ignore the pixel values by creating a binary map $C_g(i,j)$:

$$C_g(i,j) = \begin{cases} 1 & \text{if } I_{in}(i,j,2) \geq t_1(i,j) \\ 0 & \text{otherwise} \end{cases} \tag{4}$$

$$t_1(i,j) = \frac{I_{in}(i,j,1) + I_{in}(i,j,3)}{2}, \tag{5}$$

where $I(i,j,1)$, $I(i,j,2)$ and $I(i,j,3)$ are the red, green and blue pixel intensities at pixel location (i,j) for an image I. Here we use the average of red and blue intensity values as the threshold for the green intensity.

- If the red channel intensity is greater than the red channel threshold $t_2(i,j)$, we ignore the pixel values by creating a binary map $C_r(i,j)$:

$$C_r(i,j) = \begin{cases} 1 & \text{if } I_{in}(i,j,1) \geq t_2(i,j) \\ 0 & \text{otherwise} \end{cases} \tag{6}$$

$$t_2(i,j) = \frac{I_{in}(i,j,2) + I_{in}(i,j,3)}{2} \tag{7}$$

So far, we have three binary maps for identifying irrelevant regions for WBC boundary segmentation, i.e, the nucleus region map $C_n(i,j)$ and the two color-based binary maps $C_g(i,j)$ and $C_r(i,j)$. In the following sections, we will ignore the edge detection results in these regions unless otherwise specified. This will help us focus on the outer boundary of the cells and remove as much noise as possible. In addition, we note that the preprocessing steps above are necessary for both the rapid staining and standard staining images.

3) MODEL FITTING FOR CELL BOUNDARY DETECTION

Now we move on to the most important step in applying our geometry constraint, as illustrated in the lower part of Fig. 1. We begin with applying a Canny edge detector [31] on the input image, and removing edge detection results from the nucleus region $C_n(i,j)$ as well as from the two color-induced background maps $C_g(i,j)$ and $C_r(i,j)$. Still, there remains a large amount of noisy edges within the cell, as shown in Fig. 3. For the sake of simplicity, for any given cell we simply search for the largest connected component [24], as

this boundary fragment typically belongs to the outer boundary of the cell. Further, if this boundary fragment has a gap, we propose a robust model fitting approach below to recover the boundary from partial observations.

Our proposed model fitting strategy is inspired by RANSAC. The proposed strategy aims to find the most appropriate model from a set of data with outliers present. Note that, after Canny edge detection, the WBC boundary has a large number of irregular and approximately circular edge pixels. Thus, we treat each pixel as a data point, and then find the two breakpoints (i.e., endpoints of the boundary fragment). In order to fit a circle that could complete the gap, we need one additional point. As shown in Fig. 3, most data points left now are inliers, so sampling only a small number of data points will be sufficient to search for a high quality model hypothesis. The main steps of the proposed model fitting strategy are described as follows:

- Search for the two breakpoints from the largest connected component of the Canny edge detection results.
- Randomly sample data points, and together with the two breakpoints, to generate circle candidates. Then we choose the best circle with the largest number of inliers from the generated candidates. The number of inliers for the generated circle candidates is computed as follows:

$$S(\theta) = \sum_{i=1}^{n} |d(x_i, \theta) < \xi|, \tag{8}$$

  where n is the number of data points, ξ is the inlier noise scale, and $d(x_i, \theta)$ is the residual value between a data point x_i and a circle θ.
- Use the breakpoints to cut the best circle hypothesis into two arcs and keep the appropriate arc. Specifically, we connect the two breakpoints with a line segment and find the midpoint, and then draw a line orthogonal to this line segment from this midpoint. In this way, the arc that should be removed will intersect with the orthogonal line at the same side as the Canny detected boundary fragment. See Fig. 3 for an illustration.
- Stitch the arc with the Canny detected boundary fragment, to obtain a complete outer boundary of a cell.

One of the key advantages of our method is that we can find the arc that best fits the gap in the boundary fragment, and then stitch the arc to the detected boundary. In this way, the pixel-accurate edge detection results will not be altered, and gaps will be filled. It should be noted that the main limitation of the original RANSAC, if applied in this step, would produce near-perfect circular segmentation, which is not the common case for WBCs. See Fig. 5 for a comparison.

IV. EXPERIMENTAL RESULTS

In this section, we compare the proposed WBC segmentation algorithm with several well-established WBC segmentation methods, including Support Vector Machine (SVM) [3], Watershed Segmentation (WS) [14], Combination Graph Segmentation (CGS) [8] and Adaptive Histogram Threshold segmentation (AHT) [9]. Firstly, we introduce the dataset and evaluation criteria. Then, we analyze the proposed algorithm by comparing the most popular model fitting algorithm (i.e., RANSAC) with our method. Afterwards, we show the qualitative and quantitative experimental results obtained by all competing methods.

A. DATASET AND EVALUATION CRITERIA

To better evaluate the algorithm in terms of accuracy and robustness, we evaluate the performance of our algorithm on two datasets (i.e., Rapid Data and Standard Data). Rapid Data contains 138 single WBC images which have a size of 120×120 under rapid staining provided by Jiangxi Tecom Science Corporation, China. Standard Data was provided by the Third People's Hospital of Fujian Province under standard staining conditions using standard staining containing 28 single WBC images, which was a size of 250×250. The experimental results of the two datasets under two dyeing conditions is able to verify the robustness of the WBC segmentation method. Two examples of the two datasets are shown in Fig. 4.

For evaluation metrics, we use four metrics: misclassification error (ME) [32], false positive rate (FPR) [33], [34] and false negative rate (FNR) [35], kappa index (KI) [36]. Lower ME, FPR, and FNR values indicate better segmentation; in contrast, higher KI values indicate better segmentation. The experiments are conducted on a laptop with 2.40GHz Intel Pentium 2020M CPU and 8GB memory, with MATLAB codes.

$$ME = 1 - \frac{|B_s \cap B_a| + |F_t \cap F_a|}{|B_s| + |F_t|} \tag{9}$$

$$FPR = \frac{|B_s \cap F_a|}{|B_s|} \tag{10}$$

$$FNR = \frac{|F_t \cap F_a|}{|F_t|} \tag{11}$$

$$KI = 2 \times \frac{F_t \cap F_a}{|F_t| + |F_a|} \tag{12}$$

Among them, B_s and F_t are the background and foreground of the ground-truth; B_a and F_a are the background and foreground of the segmentation results.

B. ALGORITHM ANALYSIS

In this work, we introduce a modified RANSAC-based model fitting method to solve WBC segmentation. However, RANSAC can be directly used to detect the cells by fitting a circle from the Canny detected boundary fragment. Specifically, we implement a naive baseline that superimpose the fitted circle onto the edge detection results. However, although RANSAC can fit the periphery of WBCs more accurately, the pixel-accurate edge detection results will be compromised for a better overall fitting. We show the qualitative results obtained by RANSAC and the proposed model fitting strategy in Fig. 5. We can see that, the outer boundary estimated by RANSAC is usually over- or under-segmented. In contrast, the proposed model fitting strategy is able to obtain a superior

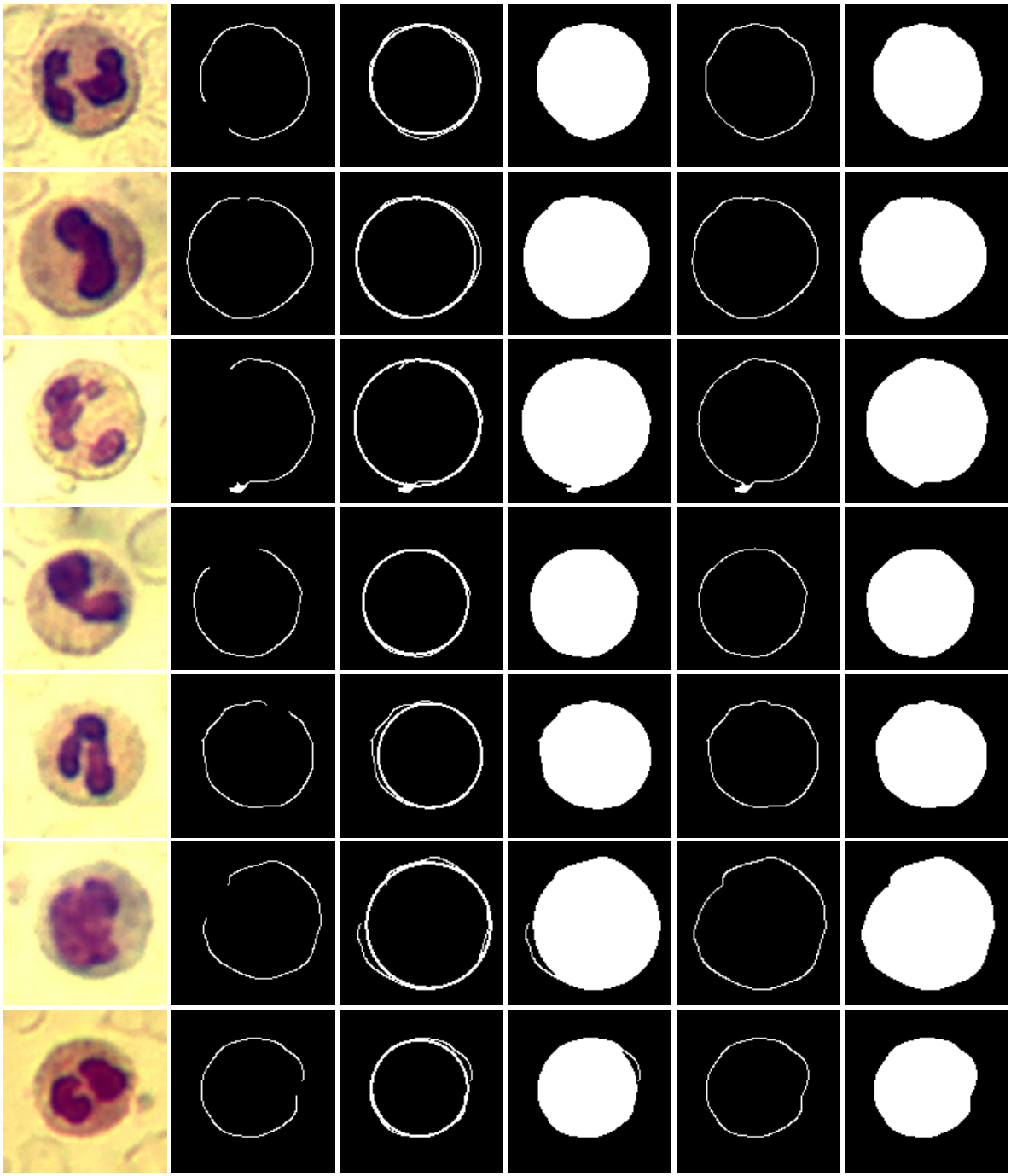

FIGURE 5. The fitting results obtained by RANSAC and the proposed model fitting strategy. (a) Original image; (b) Edge detection image; (c) and (d) The circle and cell estimated by RANSAC; (e) and (f) The circle and cell estimated by the proposed model fitting strategy.

performance, and the results better align with ground-truth cell boundaries.

C. QUALITATIVE ANALYSIS

We first present some intuitive results on the WBC segmentation of our algorithm. We randomly select eight images and present the segmentation results of each algorithm from the rapid staining data and standard staining data. The segmentation results of two different datasets obtained by all competing algorithms are shown in Fig. 6 and Fig. 7, respectively. We can see that, the proposed algorithm is significantly better than the SVM segmentation algorithm, the Watershed Segmentation algorithm (WS), and the Combined Graph Segmentation algorithm (CGS). For WS and CGS, they

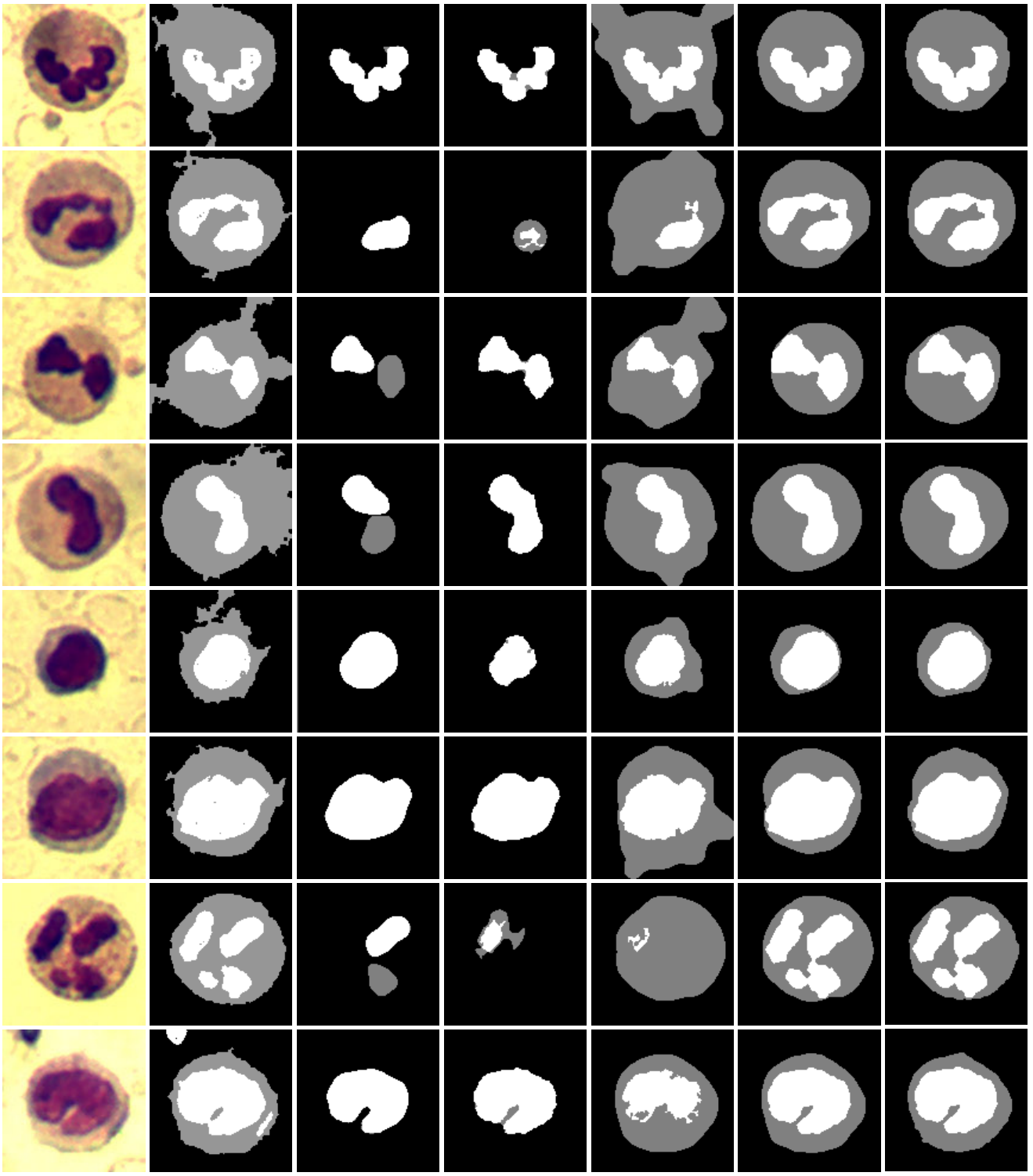

FIGURE 6. Experimental results obtained by different algorithms for Rapid Data. (a) Original images. (b)-(e) The segmentation results obtained by SVM, WS, CGS and the proposed algorithm, respectively. (f) Ground truth.

frequently mistake the nucleus for the entire cell. In contrast, SVM and AHT frequently mistake the cell for the background or RBCs. Although AHT is more accurate, it also mistakes the nucleus for the entire cell in some cases. Combining the results illustrated in Fig. 6 and Fig. 7, we can see that the proposed algorithm leads to the most accurate segmentation results compared to the above mentioned methods.

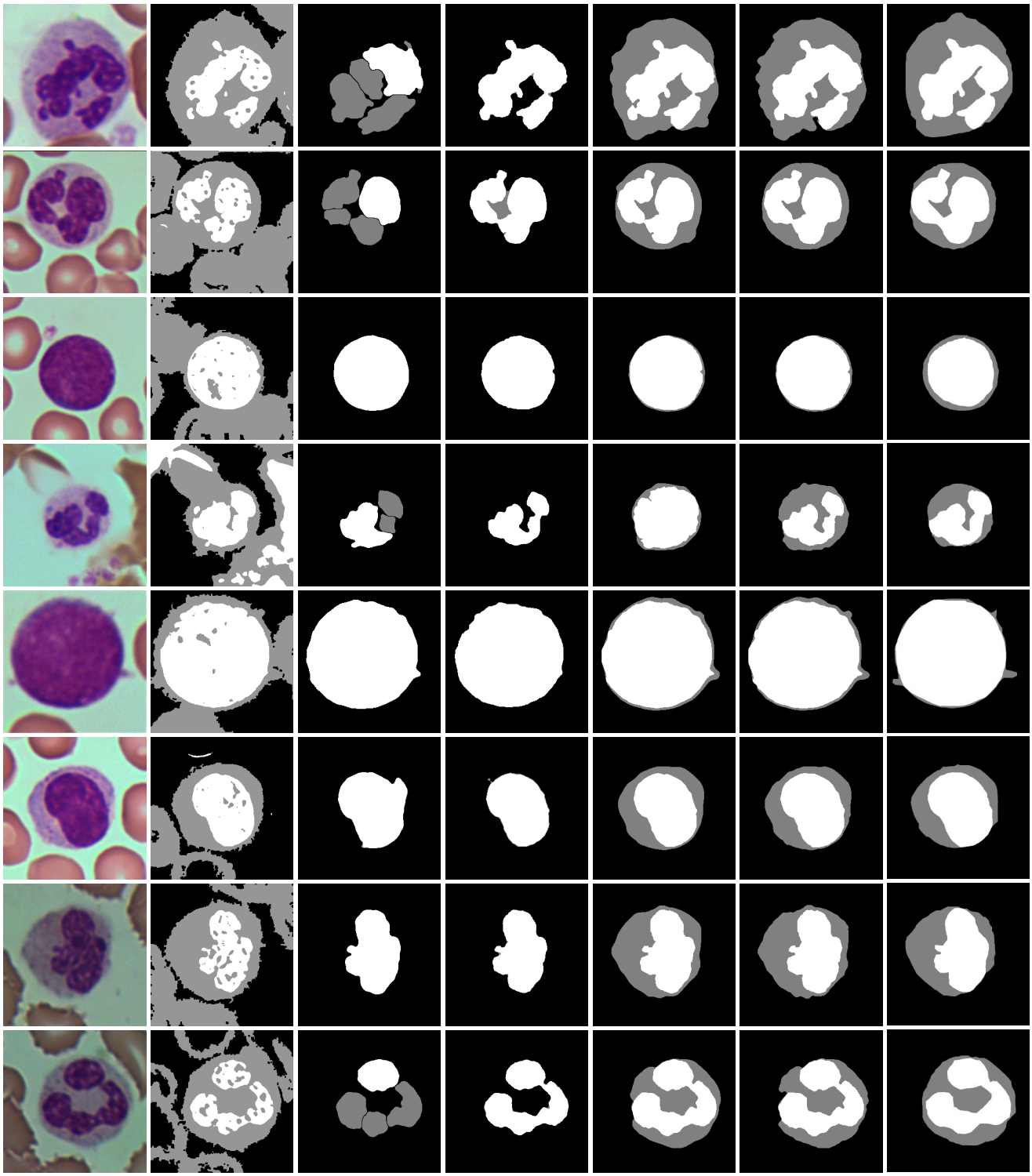

FIGURE 7. Experimental results obtained by different algorithms for Standard Data. (a) Original images. (b)-(e) The segmentation results obtained by SVM, WS, CGS and the proposed algorithm, respectively. (f) Ground truth.

D. QUANTITATIVE ANALYSIS

To provide quantitative comparisons, we compare the proposed algorithm with four state-of-the-art WBC segmentation methods: CGS [8], WS [14], SVM [3] and AHT [9]. We report the ME, FPR, FNR, KI (lower ME indicates more accurate segmentation results, and higher

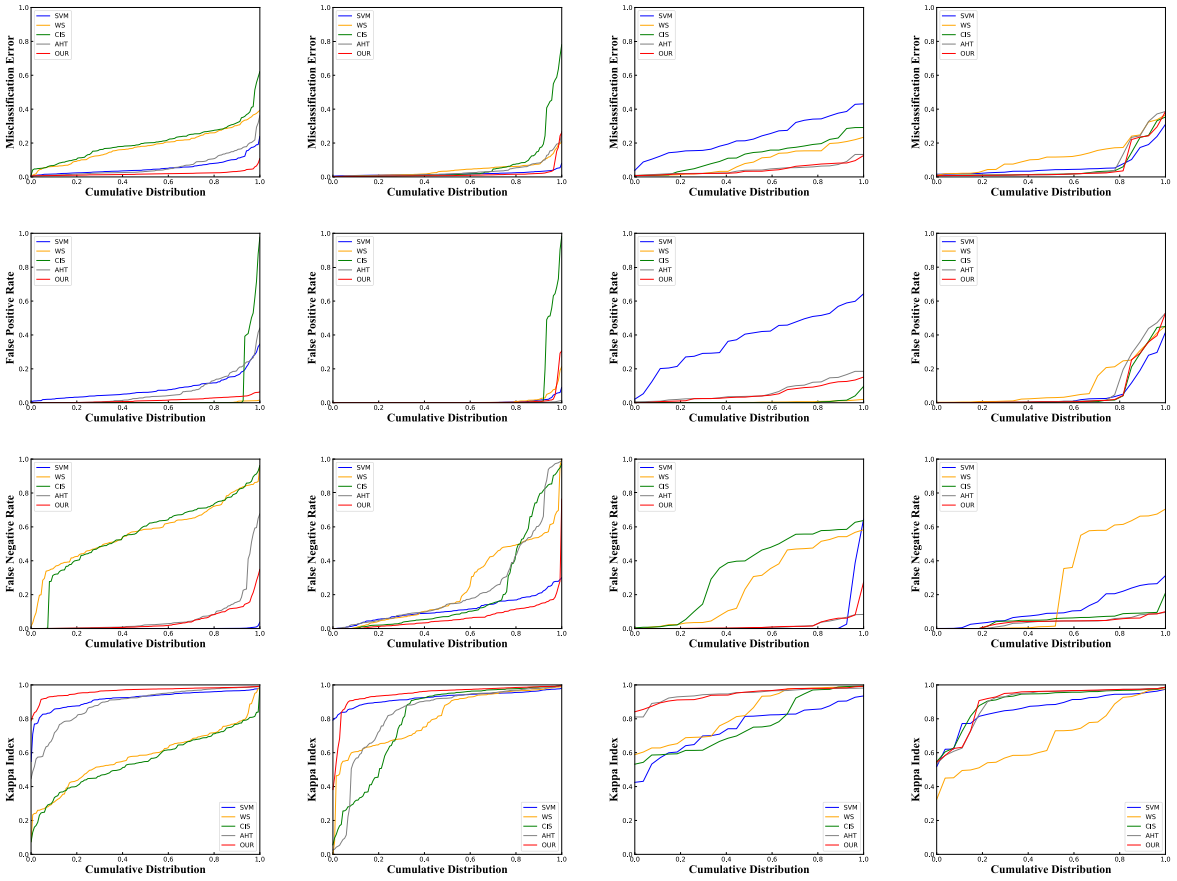

FIGURE 8. Quantitative comparison on two datasets. From top to bottom: Cumulative distributions of ME, FPR, FNR and KI. From left to right: Results on the cell in Rapid Data (a), the nucleus in Rapid Data (b), the cell in Standard Data (c) and the nucleus in Standard Data (d). Four WBC segmentation algorithms (i.e., CGS, WS, SVM and AHT) and the proposed algorithm are used for a comparison.

TABLE 1. Average values of ME, FPR, FNR and KI obtained by SVM, WS, CIS, AHT and the proposed algorithm on Rapid Data and Standard Data. The best results are boldfaced.

Data	Method	ME	FPR	FNR	KI
Rapid Data (cell)	SVM	0.0555	0.0830	**0.0009**	0.9179
	WS	0.1828	**0.0013**	0.5678	0.5797
	CIS	0.2055	0.0427	0.5583	0.5522
	AHT	0.0641	0.0662	0.0686	0.8885
	OUR	**0.0197**	0.0154	0.0422	**0.9629**
Rapid Data (Nucleus)	SVM	0.0184	0.0053	0.1130	0.9250
	WS	0.0421	0.0099	0.2472	0.8048
	CIS	0.0695	0.0501	0.2098	0.7918
	AHT	0.0355	**0.0007**	0.2410	0.8239
	OUR	**0.0160**	0.0084	**0.0666**	**0.9451**
Standard Data (cell)	SVM	0.2380	0.3741	0.0379	0.7467
	WS	0.0936	**0.0042**	0.2595	0.8290
	CIS	0.1286	0.0063	0.3524	0.7612
	AHT	0.0448	0.0667	**0.0165**	0.9439
	OUR	**0.0425**	0.0537	0.0240	**0.9443**
Standard Data (Nucleus)	SVM	0.0656	**0.0541**	0.1150	0.8591
	WS	0.1278	0.1061	0.2723	0.6883
	CIS	0.0617	0.0674	0.0548	0.8994
	AHT	0.0722	0.0871	**0.0380**	0.8939
	OUR	**0.0615**	0.0709	0.0395	**0.9008**

KI indicates more accurate segmentation results) obtained by all the five competing algorithms in Fig. 8 and Table 1. We can see that two competing methods (i.e., SVM and the proposed algorithm) are able to achieve low ME and high KT on the cells from the Rapid Data than the other three competing methods. However, SVM often mistakes the cell for the background. Therefore, its FPR is the highest, and the FNR is the lowest on the Rapid Data (cell). Our proposed algorithm, on the other hand, distinguishes the cell and the background by a geometry constraint, and obtains more accurate segmentation results. For the nucleus of the Rapid Data, SVM has a lower ME than WS, CIS and AHT. The proposed algorithm, however, has an even lower ME and a higher KI (i.e., more accurate than the SVM). Note that AHT has a lower FNR than the proposed algorithm due to its over-segmentation. For the Standard Data with many RBCs that have similar nuclei and cytoplasms compared to WBCs, we can see that AHT and the proposed algorithm have a higher KI and a lower ME. AHT uses the morphological operations, which often result in over-segmentations. The proposed algorithm is able to achieve better performance thanks to the geometry constraint. For the nucleus of the Standard Data, we can see that AHT and the proposed algorithm achieve better performance than other three algorithms. It is worth pointing out that the proposed algorithm is based on a sparse image representation which can reduce unimportant features. Therefore, our algorithm has a lower ME and higher KI than AHT.

V. CONCLUSION

In this paper, we introduce sparsity and geometry constraints to detect nuclei and cells for WBC segmentation. Specifically, we first construct a sparse image representation and then segment the nuclei with a sparsity constraint. The constructed sparse image representation is able to remove background and RBC by combining the information from the HSL color space and the RGB color channels. To improve the robustness to outliers, we further propose a novel model fitting strategy (i.e., the geometric constraint) to detect outer cell boundaries. The experimental results on two datasets that include both rapid and standard staining images verify the effectiveness of the proposed algorithm. In the future, we would like to explore more challenging cases such as the segmentation of multiple cells and cells of multiple classes.

REFERENCES

[1] F. Xing and L. Yang, "Robust nucleus/cell detection and segmentation in digital pathology and microscopy images: A comprehensive review," *IEEE Rev. Biomed. Eng.*, vol. 9, pp. 234–263, Jan. 2016.

[2] W. Shitong, K. F. L. Chung, and F. Duan, "Applying the improved fuzzy cellular neural network IFCNN to white blood cell detection," *Neurocomputing*, vol. 70, nos. 7–9, pp. 1348–1359, 2007.

[3] X. Zheng, Y. Wang, and G. Wang, "White blood cell segmentation using expectation-maximization and automatic support vector machine learning," *Data Acquisition Process*, vol. 28, no. 5, pp. 614–619, 2013.

[4] O. Ronneberger, P. Fischer, and T. Brox, "U-net: Convolutional networks for biomedical image segmentation," in *Proc. Int. Conf. Med. Image Comput. Comput.-Assist. Intervent.*, 2015, pp. 234–241.

[5] V. Badrinarayanan, A. Kendall, and R. Cipolla, "SegNet: A deep convolutional encoder-decoder architecture for image segmentation," *IEEE Trans. Pattern Anal. Mach. Intell.*, vol. 39, no. 12, pp. 2481–2495, Dec. 2017.

[6] J. Long, E. Shelhamer, and T. Darrell, "Fully convolutional networks for semantic segmentation," in *Proc. IEEE Conf. Comput. Vis. Pattern Recognit.*, Jun. 2015, pp. 3431–3440.

[7] L. H. Nee, M. Y. Mashor, and R. Hassan, "White blood cell segmentation for acute leukemia bone marrow images," *J. Med. Imag. Health Inform.*, vol. 2, no. 3, pp. 278–284, 2012.

[8] D. Gu and G. Cui, "Flexible combination segmentation algorithm for leukocyte images," *Chin. J. Sci. Instrum.*, vol. 29, no. 9, pp. 1977–1981, 2008.

[9] X. Zhou, C. Wang, Z. Li, and F. Zhang, "Adaptive histogram thresholding-based leukocyte image segmentation," in *Advances in Intelligent Information Hiding and Multimedia Signal Processing* (Smart Innovation, Systems and Technologies), vol. 157, J. S. Pan, J. Li, P. W. Tsai, and L. Jain, Eds. Singapore: Springer, 2020, doi: 10.1007/978-981-13-9710-3_47.

[10] C. Zhang, X. Xiao, X. Li, Y.-J. Chen, W. Zhen, J. Chang, C. Zheng, and Z. Liu, "White blood cell segmentation by color-space-based k-means clustering," *Sensors*, vol. 14, no. 9, pp. 16128–16147, 2014.

[11] B. J. Ferdosi, S. Nowshin, F. A. Sabera, and Habiba, "White blood cell detection and segmentation from fluorescent images with an improved algorithm using k-means clustering and morphological operators," in *Proc. Int. Conf. Elect. Eng. Inf. Commun. Technol.*, Sep. 2018, pp. 566–570. [Online]. Available: https://ieeexplore.ieee.org/document/8628068

[12] N. Theera-Umpon, "White blood cell segmentation and classification in microscopic bone marrow images," in *Proc. Int. Conf. Fuzzy Syst. Knowl. Discovery*, 2005, pp. 787–796.

[13] Z. Liu, J. Liu, X. Xiao, H. Yuan, X. Li, J. Chang, and C. Zheng, "Segmentation of white blood cells through nucleus mark watershed operations and mean shift clustering," *Sensors*, vol. 15, no. 9, pp. 22561–22586, 2015.

[14] S. Arslan, E. Ozyurek, and C. Gunduz-Demir, "A color and shape based algorithm for segmentation of white blood cells in peripheral blood and bone marrow images," *Cytometry A*, vol. 85, no. 6, pp. 480–490, 2014.

[15] X. Zheng, Y. Wang, G. Wang, and J. Liu, "Fast and robust segmentation of white blood cell images by self-supervised learning," *Micron*, vol. 107, pp. 55–71, Apr. 2018.

[16] M. Habibzadeh, M. Jannesari, Z. Rezaei, H. Baharvand, and M. Totonchi, "Automatic white blood cell classification using pre-trained deep learning models: ResNet and inception," in *Proc. 10th Int. Conf. Mach. Vis. (ICMV)*, vol. 10696, 2018, p. 1069612.

[17] P. Tiwari, J. Qian, Q. Li, B. Wang, D. Gupta, A. Khanna, J. J. Rodrigues, and V. H. C. de Albuquerque, "Detection of subtype blood cells using deep learning," *Cogn. Syst. Res.*, vol. 52, pp. 1036–1044, Dec. 2018.

[18] A. I. Shahin, Y. Guo, K. M. Amin, and A. A. Sharawi, "White blood cells identification system based on convolutional deep neural learning networks," *Comput. Methods Programs Biomed.*, vol. 168, pp. 69–80, Jan. 2017.

[19] M. I. Razzak and S. Naz, "Microscopic blood smear segmentation and classification using deep contour aware CNN and extreme machine learning," in *Proc. IEEE Conf. Comput. Vis. Pattern Recognit. Workshops (CVPRW)*, Jul. 2017, pp. 801–807.

[20] J. W. Choi, Y. Ku, B. W. Yoo, J.-A. Kim, D. S. Lee, Y. J. Chai, H.-J. Kong, and H. C. Kim, "White blood cell differential count of maturation stages in bone marrow smear using dual-stage convolutional neural networks," *PLoS ONE*, vol. 12, no. 12, 2017, Art. no. e0189259.

[21] K. Jiang, Q.-M. Liao, and Y. Xiong, "A novel white blood cell segmentation scheme based on feature space clustering," *Soft Comput.*, vol. 10, no. 1, pp. 12–19, 2006.

[22] G. H. Joblove and D. Greenberg, "Color spaces for computer graphics," *ACM SIGGRAPH Comput. Graph.*, vol. 12, no. 3, pp. 20–25, Aug. 1978.

[23] P. K. Sahoo, S. Soltani, and A. K. C. Wong, "A survey of thresholding techniques," *Comput. Vis., Graph., Image Process.*, vol. 41, no. 2, pp. 233–260, 1998.

[24] D. G. Bailey and C. T. Johnston, "Single pass connected components analysis," in *Proc. Image Vis. Comput. New Zealand*, 2007, pp. 282–287.

[25] G. Xiao, H. Wang, Y. Yan, and D. Suter, "Superpixel-guided two-view deterministic geometric model fitting," *Int. J. Comput. Vis.*, vol. 127, no. 4, pp. 323–339, 2019.

[26] G. Xiao, H. Wang, Y. Yan, and L. Zhang, "Robust geometric model fitting based on iterative hypergraph construction and partition," *Neurocomputing*, vol. 336, pp. 56–66, Apr. 2019.

[27] J. Ma, X. Jiang, J. Jiang, J. Zhao, and X. Guo, "LMR: Learning a two-class classifier for mismatch removal," *IEEE Trans. Image Process.*, vol. 28, no. 8, pp. 4045–4059, Aug. 2019.

[28] J. Ma, J. Zhao, J. Jiang, H. Zhou, and X. Guo, "Locality preserving matching," *Int. J. Comput. Vis.*, vol. 127, no. 5, pp. 512–531, 2019.

[29] H. Wang, G. Xiao, Y. Yan, and D. Suter, "Searching for representative modes on hypergraphs for robust geometric model fitting," *IEEE Trans. Pattern Anal. Mach. Intell.*, vol. 41, no. 3, pp. 697–711, Mar. 2018.

[30] M. A. Fischler and R. Bolles, "Random sample consensus: A paradigm for model fitting with applications to image analysis and automated cartography," *Commun. ACM*, vol. 24, no. 6, pp. 381–395, 1981.

[31] J. Canny, "A computational approach to edge detection," *IEEE Trans. Pattern Anal. Mach. Intell.*, vol. PAMI-8, no. 6, pp. 679–698, Nov. 1986.

[32] W. A. Yasnoff, J. K. Mui, and J. W. Bacus, "Error measures for scene segmentation," *Pattern Recognit.*, vol. 9, no. 4, pp. 217–231, 1977.

[33] L. Wei, P. Xing, J. Zeng, J. Chen, R. Su, and F. Guo, "Improved prediction of protein–protein interactions using novel negative samples, features, and an ensemble classifier," *Artif. Intell. Med.*, vol. 83, pp. 67–74, Nov. 2017.

[34] L. Wei, S. Wan, J. Guo, and K. K. L. Wong, "A novel hierarchical selective ensemble classifier with bioinformatics application," *Artif. Intell. Med.*, vol. 83, pp. 82–90, Nov. 2017.

[35] J. L. Fleiss, J. Cohen, and B. S. Everitt, "Large sample standard errors of kappa and weighted kappa," *Psychol. Bull.*, vol. 72, no. 5, pp. 323–327, 1969.

[36] T. Fawcett, "An introduction to ROC analysis," *Pattern Recognit. Lett.*, vol. 27, no. 8, pp. 861–874, Jun. 2006.

ZHEN ZHONG received the bachelor's degree in traditional Chinese medicine from the Hunan University of Chinese Medicine, Hunan, China, in 2018. He is currently pursuing the M.S. degree with the Department of Traditional Chinese Medicine, Fujian University of Traditional Chinese Medicine, where he is also attached to the Fujian Provincial Key Laboratory of Information Processing and Intelligent Control, Minjiang University. His research interests include computer vision, machine learning, and pattern recognition.

TAO WANG received the B.E. degree in information engineering from the South China University of Technology, Guangzhou, China, in 2009, and the Ph.D. degree in computer science from The Australian National University, Canberra, ACT, Australia, in 2016. He was a member of the Computer Vision Research Group, National ICT Australia, Canberra. He is currently a Lecturer with the College of Computer and Control Engineering, Minjiang University, Fuzhou, China. He is also with the College of Mathematics and Computer Science, Fuzhou University, Fuzhou, and NetDragon Inc., Fuzhou. His research interests include scene understanding, object detection, and semantic instance segmentation.

KUN ZENG received the Ph.D. degree from the Department of Computer Science, Xiamen University, Xiamen, China, in 2015. He was a Postdoctoral Fellow with the Department of Electronic Science, Xiamen University, from 2016 to 2019. He is currently a Lecturer with Minjiang University, China. His current research interests include image processing, machine learning, and medical image reconstruction.

XIAOGEN ZHOU is currently pursuing the M.S. degree with the College of Mathematics and Computer Science, Fuzhou University, Fuzhou, China. His current research interests include pattern recognition, machine learning, and digital signal processing.

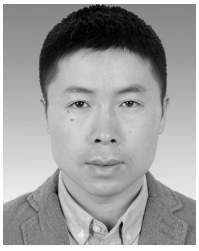

ZUOYONG LI received the B.S. and M.S. degrees in computer science and technology from Fuzhou University, Fuzhou, China, in 2002 and 2006, respectively, and the Ph.D. degree from the School of Computer Science and Technology, Nanjing University of Science and Technology (NUST), Nanjing, China, in 2010. He is currently a Professor with the College of Computer and Control Engineering, Minjiang University, Fuzhou, where he is also an Adjunct Principal Investigator with the Department of Traditional Chinese Medicine, Fujian University of Traditional Chinese Medicine. He has published over 60 articles in international/national journals. His current research interests include image processing, pattern recognition, and machine learning.